



Design and development of TiO₂-Fe⁰ nanoparticle-immobilized nanofibrous mat for photocatalytic degradation of hazardous water pollutants

Hridam Deb^{1,2} · Mohammad Neaz Morshed¹ · Shili Xiao¹ · Shamim Al Azad³ · Zhicheng Cai¹ · Arsalan Ahmed²

Received: 15 December 2018 / Accepted: 19 January 2019 / Published online: 29 January 2019
© Springer Science+Business Media, LLC, part of Springer Nature 2019

Abstract

This study introduces, a titanium dioxide (TiO₂) and zerovalent iron (Fe⁰) nanoparticles immobilized electrospun poly (acrylic acid)/poly (vinyl alcohol) (PAA/PVA) nanofibrous mat for photocatalytic degradation of hazardous water pollutant. For that, PAA/PVA nanofibrous mat was prepared by electrospinning followed by crosslinking and immobilization/incorporation of TiO₂ and Fe⁰ nanoparticles through Layer-by-Layer (LbL) self-assembly method. The obtained PAA/PVA-TiO₂ and PAA/PVA-TiO₂-Fe⁰ was fully characterized by scanning electron microscopy (SEM), FTIR, TGA and porosity analysis. The results showed successful immobilization of both (TiO₂ and Fe⁰) nanoparticles on the nanofibrous mat with uniform distribution. The latter exhibited catalytic activity towards the degradation of Methyl Blue (MB) and Brilliant Green (BG) dyes separately and mixed in the presence of UV light. UV-Vis spectroscopic analysis was used to monitor and quantitative analysis of the degradation. It has been found that high photocatalytic activity of the functional nanofibrous mats has been observed. The fastest conversion rate reached to 99.2% in 20 min at a rate constant of 0.0847/min providing adequate reusability of the nanofiber mats up to four consecutive cycles. A mechanism of the photocatalytic activities has been proposed by referring to the above results. The results opened a promising prospect for using nanofibrous based effective photocatalyst for environmental application.

1 Introduction

A major environmental issue resides undoubtedly in water pollution, more particularly by aromatic compounds (organic dyes, phenols, pesticides, drugs and hormone disrupters), heavy metal ions and bacterial agents [1–3] are being released in water sources [4–6]. The toxicity, stability to natural decomposition and persistence in the environment of these are the cause of much concern to

societies and regulatory authorities around the world [7]. An enormous number of water treatment technologies based on both physical and chemical processes has been proposed [8]. Some of those processes incorporated nanotechnology and nanomaterials for coagulation, flocculation, adsorption and/or catalysts (such as photocatalysis) [9, 10]. Among them, photocatalysis revealed its potentiality as a promising method for sustainable water treatment [11]. However, the physicochemical properties of photocatalysts are strongly important for the effectiveness of the system which depends on their structure, morphology and specific surface area of the material used [12]. A wide variety of coupled nanomaterials such as ZnO-TiO₂, CuO-ZnO, CuO-TiO₂, CuO-SnO₂, TiO₂-SnO₂, ZnO-SnO₂ and so on have been introduced as a great interest of many water researchers [13–22]. However, TiO₂ based photo-catalysis has been proven as a fascinating cut-rate approach for the degradation and demineralization of persistent pollutants (such as dyestuffs) of wastewater [23, 24]. During last few decades, TiO₂ shows the versatility of application in the material science and engineering involves doping [25], coupling [26], capping [27], dye

✉ Mohammad Neaz Morshed
engr.neazmorshed@yahoo.com

✉ Shili Xiao
xshili@yahoo.com

¹ State Key Laboratory of New Textile Materials and Advanced Technology, School of Textile Science and Engineering, Wuhan Textile University, Wuhan 430200, Hubei, China

² College of Materials and Textiles, Zhejiang Sci-Tech University, Hangzhou 310018, Zhejiang, China

³ College of Chemistry and Chemical Engineering, Wuhan Textile University, Wuhan 430200, Hubei, China

sensitization [28], pesticide removal [29] and photo-catalytic property to degradation of numerous organic contaminants [30–32]. However, Many studies have demonstrated that the efficiency of TiO_2 can be increased by the addition of dissolved transition metals such as Fe, Ni, Mn, Co and Cu [33–35] and carbon nanotube [36]. Some researchers have developed composites of TiO_2 and metal oxides and have discovered that the photocatalytic ability of the composites was better than those of the combined effect of TiO_2 and soluble metal ions due to its faster chemical reaction. Reportedly, zerovalent iron nanoparticles (ZVI NPs) and their nanobimetallic systems (Fe/Pd) [37, 38], Fe/Ni [39–41], Fe/Ag [42] exhibited superior capacity in the catalytic degradation of toxic pollutants including; trichloroethylene (TCE) and polychlorinated biphenyls (PCBs) [37, 43, 44], sequestration of toxic metal ions such as As(V) [45] and Cr(VI) [46], in the stabilization of biosolids [47], in the decoloration of dyes [48, 49], and in the degradation of nuclear wastes [50], explosives [51], and herbicides [52].

Apart from all these positive aspects, there is a concerning issue that limits their potential industrial application. The catalyst particles that catalyzed by photons need to be separated and recycled before discharging the treated wastewater so can be defined as a time-killing procedure. Moreover, the catalyst particles possess a high amount of absorption capability causing the poor intensity of penetration of UV light [53, 54]. So, immobilization of catalyst may come across as appropriate remediation for this crisis. Several researchers introduced different immobilization technique for durable deposition and sustainable applicability includes, Layer-by-Layer (LbL) [55], adsorption [56], crosslinking [57], atomic layer deposition [58] etc. Various materials such as zeolites [59], clays [60], textiles [21] and inorganic–organic materials have been applied as supports for metallic nanoparticles in diverse catalytic reactions [61, 62]. Up to now, these materials have attracted much attention due to their availability and effectiveness towards potential applications, particularly in the field of catalysis [63–66]. Interestingly among all those materials, special features of porous materials become an ideal supporting matrix for metal nanoparticles [67–69]. As a matter of fact, higher porosity of the material leads to superior competence.

Extraordinary features like as small diameters in the range of nanometers to a few microns, high aspect ratio, and the high specific surface area, polymeric electrospun nanofibrous and nanostructured inorganic/polymer composite materials has gained enormous interest as a support material for robust immobilization of different organic and inorganic materials [70, 71]. Thus we design and developed nanofibrous mats immobilized with TiO_2/Fe nanoparticles as a novel photo-catalyst for catalytic degradation

of toxic water pollutants. It is estimated that the result, stability and effectiveness of the designed functional nanofibrous mat will open a broad range of application of nanofibrous based photo-catalysts for superior environmental remediation.

2 Experimental

2.1 Chemicals

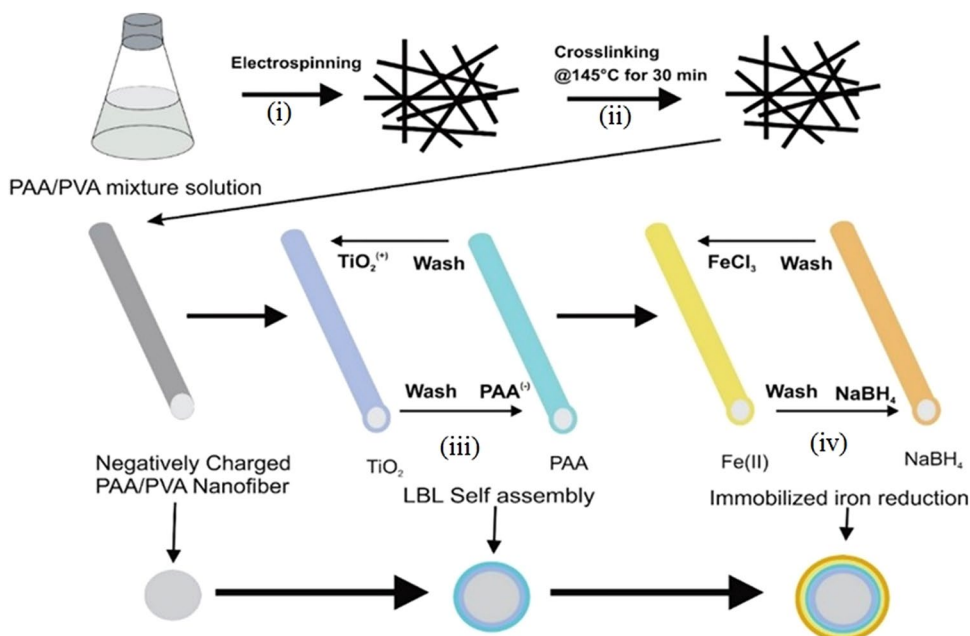
PAA (average Mw-240,000, 25% in water) was obtained from Acros Organics. PVA (88% hydrolyzed, average Mw-8800) and Sodium Borohydride (NaBH_4) (Mw-37.83) and TiO_2 (Mw-79.87) were from Aladdin Industrial Corporation, China and Ferric Chloride ($\text{FeCl}_3 \cdot 6\text{H}_2\text{O}$) (Mw-270.29), Methyl Blue (MB) (average Mw-799.80) and Brilliant Green (BG) (Mw-482.63) were purchased from Sinopharm Chemical Reagent Co. Ltd. China. All chemicals were of analytical grade and used without further purification. Water used in all experiments was purified using a water purification system from Chengdu Ultra Technology Co., Ltd. China (ULUPURE Model: UPH-II-20T) with a resistivity higher than 18 M Ω cm.

2.2 Preparation, functionalization, and design of PAA/PVA– TiO_2 – Fe^0

Scheme 1 illustrates the methods used for preparation and development of functional nanofibrous mat. The process mainly consisted of the following steps:

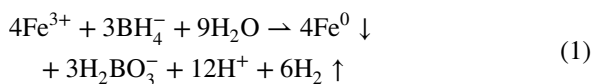
- (a) Electrospun poly (acrylic acid)/poly (vinyl alcohol) (PAA/PVA) nanofibrous mats were fabricated by laboratory-based electrospinning arrangement as described in our previous reports [72, 73]. Typically, 10 wt% PAA/PVA mixture solution was prepared by ensuring the mass ratio of the PAA and PVA polymer 1:1, considering their suitable visco-electrostatic nature [74]. The fresh PAA/PVA solution was mildly stirred and filled in a 10 mL syringe attached with a blunt steel needle (diameter of 0.8 mm). The extrusion speed of the syringe was 0.5 mL/h. A high voltage of power (16.6 kV) was connected between a grounded aluminium board (collector) and syringe-capillary to produce sufficient drift velocity to overcome electrostatic repulsion of charged space and could be collected on the aluminium foil. The distance between the syringe-capillary and collector was kept 25 cm. The freshly prepared PAA/PVA nanofiber mats were dried overnight.
- (b) Then the nanofiber mats were crosslinked using thermal treatment in a vacuum dryer at a temperature of 145 °C

Scheme 1 Functionalization route of PAA/PVA nanofibrous mats via (i) Electrospinning, (ii) Crosslinking, (iii) Immobilization of TiO₂ nanoparticles and, (iv) Incorporation of zerovalent iron nanoparticles



for 30 min to provide water insolubility of the nanofiber mats [75].

- (c) In order to ensure uniform and robust grafting of metal nanoparticles, PAA/PVA nanofibrous mats were prone to (LbL) immobilization of TiO₂ and Fe⁰ nanoparticles. Firstly, the water-stable PAA/PVA nanofiber mats were immersed into a solution of TiO₂ (0.375 g/L) followed by a layer of PAA in order to introduce anionic charge in the surface for subsequent exchange for cationic TiO₂ nanoparticles. With the desired immersion/rinsing cycle, the PAA/PVA–TiO₂ nanofibrous mats were prepared.
- (d) The incorporation of ZVI NPs in PAA/PVA–TiO₂ nanofibrous mats was achieved using Iron (III) chloride as precursors and sodium tetrahydroborate (0.94 mol/L, 5 mL) as a reducing agent in 100 mL of water, under stirring at room temperature for 4 h. Reaction (1) illustrates the reduction process of iron ions into ZVI NPs. The obtained product denoted as PAA/PVA–TiO₂–Fe⁰ was dried at 65 °C for several hours and then stored in a sealed enclosure containing a dried and O₂-free chamber.



2.3 Material characterizations

Both the PAA/PVA–TiO₂ and PAA/PVA–TiO₂–Fe⁰ nanofibrous mats were systematically characterized. Scanning Electron Microscope (SEM) (JSM- 6510LV, JEOL Ltd., Japan) with an operating voltage of 20 KV

was used to observe the surface morphologies of the functionalized nanofibrous mat. Freshly prepared nanofiber mats and recycled nanofibrous mats were also taken into consideration to identify morphology changes. The diameters of nanofibers were measured using image analysis software ImageJ 1.40G (<http://rsb.info.nih.gov/ij/download.html>). At least 200 randomly selected nanofibers were observed using SEM images and analyzed for each sample to obtain the diameter distribution histograms. Thermogravimetric Analysis (TGA) was performed by a TGA/SDTA851° (Mettler-Toledo Instruments Ltd. Shanghai, China) thermogravimetric analyzer with a heating rate of 10°C/min from room condition to 800 °C. To identify the functional groups within the nanofibers, FT-IR spectra were recorded using a VERTEX 70 FT-IR spectrometer (Bruker Corporation, Germany) at the wave-number range of 4000–500 cm⁻¹ at ambient condition. The apparent density and mat porosity of the nanofibers before and after treatment with Fe and TiO₂ were calculated using Eqs. (2) and (3) [76]. The thickness of the nanofibrous mat was measured by a micrometer and the bulk density of the mixture was calculated according to their weight ratio.

$$\text{Apparent density (g/cm}^3\text{)} = \frac{\text{Mat mass (g)}}{\text{Mat thickness (cm)} \times \text{Mat area (cm}^2\text{)}} \quad (2)$$

$$\text{Mat porosity} = 1 - \left(\frac{\text{Mat apparent density (g/cm}^3\text{)}}{\text{Bulk density of mixture (g/cm}^3\text{)}} \right) \times 100\% \quad (3)$$

2.4 Photocatalytic degradation of hazardous water pollutants

The photocatalytic activity of functional nanofibrous mat towards degradation of MB, BG dyes separately and mixed were investigated by using UV–Vis spectrophotometric analysis (UV-2550, Shimadzu Corporation, Japan). Degradation reactions were carried out in a 40 ml glass beaker; the concentration of mixture solution was 30 mg/L and 60 mg/L for MB and BG respectively. To the above solution, 500 mg/L of catalysts was added. Each of the reactor was magnetically stirred under a UV light source of Tungsten filament lamp of 500 W with an operational voltage of 220 V. Within several time intervals, 1 mL of fluidic sample was taken out from the reaction chamber and reserved in a transparent tube for quantitative measurement. Prior to quantitative measurement, the samples were diluted to 3 mL with demineralized water and the degradation of MB and BG was calculated according to the Eq. (4) referring the absorbance calibration curve of known standard solutions.

$$\text{Degradation\%} = \frac{C_0 - C_t}{C_0} \times 100 \quad (4)$$

Here, C_0 = Initial concentration of colorants solution, C_t = Concentration of the colorants at different time intervals.

3 Results and discussion

3.1 Morphological properties

The morphological properties of the untreated PAA/PVA, PAA/PVA–TiO₂ and PAA/PVA–TiO₂–Fe⁰ nanofibrous mats were investigated by SEM. Variations in fiber diameter have also been monitored from SEM images using ImageJ analysis as shown in Fig. 1. The untreated PAA/PVA nanofibrous mats (Fig. 1a) exhibited a random network of overlapped fibers with a fairly smooth surface. After immobilization of TiO₂ nanoparticles, a visible change in the surface showed layered clusters in the form of scale aggregates, indicating that the surface of nanofibrous mats was covered with TiO₂ nanoparticles (Fig. 1c). The same trend was obtained after incorporation of ZVI NPs (Fig. 1e). However, the incorporation of Fe⁰ nanoparticles induced a thorough change in the surface morphology of PAA/PVA–TiO₂, resulting in a smoother surface and formation of bulkier clusters of smaller particles.

Diameter distribution analysis of all fibrous mats reveals that freshly prepared crosslinked PAA/PVA nanofibers have a mean diameter of 170 ± 25 nm (Fig. 1b) which has been increased to 222 ± 42 nm in PAA/PVA–TiO₂ (Fig. 1d) and 267 ± 32 nm in PAA/PVA–TiO₂–Fe⁰ (Fig. 1f) is due to the presence of TiO₂ and Fe⁰ nanoparticles. A thin layer of TiO₂ (approx. 52 nm) and TiO₂–Fe⁰ (approx. 97 nm)

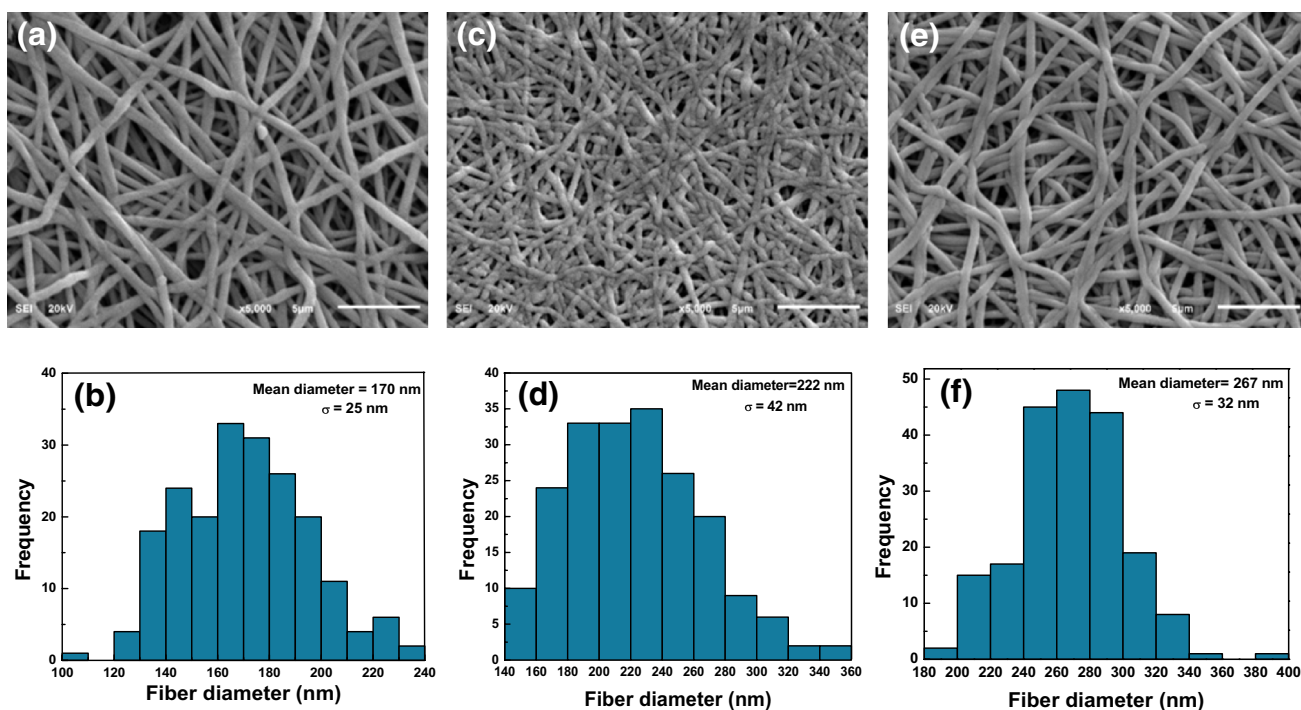


Fig. 1 SEM images and diameter distribution diagram of PAA/PVA (a, b), PAA/PVA–TiO₂ (c, d) and PAA/PVA–TiO₂–Fe⁰ (e, f) nanofibrous mat

Scheme 2 The effective immobilization of $\text{TiO}_2\text{-Fe}^0$ on the PAA/PVA nanofibrous mat

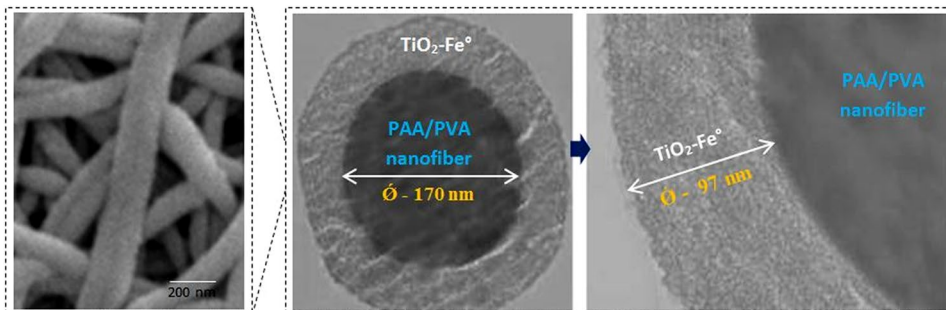


Table 1 Porosity of nanofibrous mats

| Nanofibrous mats | Porosity% |
|---|-----------|
| PAA/PVA nanofibers | 86.6 |
| Crosslinked PAA/PVA nanofibrous mats | 69.6 |
| PAA/PVA-TiO ₂ | 71.2 |
| PAA/PVA-TiO ₂ -Fe ⁰ | 73.7 |

nanoparticles have been immobilized successfully in the surface of the nanofibers through electrostatic attraction as illustrated in Scheme 2.

Since the diameter of the nanofibers varied according to the nanoparticles loading, so it is crucial to know about the fibers porosity, as it supposed to have relied on fundamental attribution for which possibility of addition or deposition of any particles or elements at the desired volume may happen. By calculating the apparent density of the nanofibers and individual bulk densities of PAA and PVA polymers, the porosity of freshly prepared PAA/PVA, Crosslinked PAA/PVA, PAA/PVA-TiO₂ and PAA/PVA-TiO₂-Fe⁰ nanofibrous mats were measured (Table 1). It has been found that the porosity of freshly prepared PAA/PVA nanofibrous mats were 86.6% which decreased to 69.6% after heat-induced cross-linking and fiber contraction thus forming the dense fibrous mats. However, further immobilization of TiO₂ and TiO₂-Fe⁰ nanoparticles decreased the porosity to 71.2% and 73.7% respectively.

It appeared that PAA/PVA nanofibers have high apparent density and porosity. However, after immobilization of TiO₂ and TiO₂-Fe⁰ nanoparticles onto the surface, porosity decreased significantly, revealing that the nanoparticles took up specific areas on the surface and porous structure of nanofibrous mat.

3.2 FT-IR chemical analysis

Infrared studies of PAA/PVA, PAA/PVA-TiO₂ and PAA/PVA-TiO₂-Fe⁰ were carried out to identify the type and natures of the functional groups shown in Fig. 2. Untreated PAA/PVA nanofibers displayed some bands in the region 3376 cm⁻¹ and 1716 cm⁻¹ ascribed to the O-H and C=O

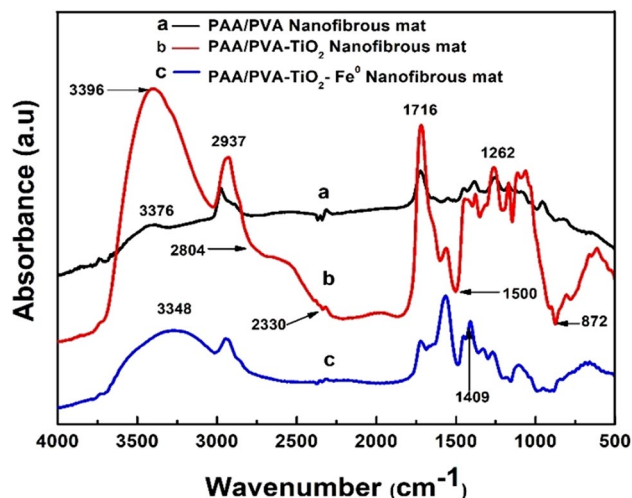


Fig. 2 FTIR spectra of untreated PAA/PVA (a), PAA/PVA-TiO₂ (b) and PAA/PVA-TiO₂-Fe⁰ nanofibrous mat

stretching vibration of PAA [77]. Due to the high-temperature thermal cross-linking of PAA/PVA nanofibers, the complementary ester bond was beyond the detection by IR spectrum as supported by the literature [78]. However, the absence of ester bond validated the claim of insolubility of nanofibrous mat.

The incorporation of TiO₂ and TiO₂-Fe⁰ over PAA/PVA nanofibrous mat introduced visible changes, as compared to the untreated mat. Upon immobilization of TiO₂ nanoparticles, the hydroxyl groups of PVA yield a sharp peak of 3396 cm⁻¹ due to the presence of a tiny amount of water molecules because of the multilayer TiO₂ assembled on the nanofibrous mat can easily absorb moisture in air while significant but reduced (3348 cm⁻¹) peak has been noticed upon Fe⁰ incorporation which is consistent with previous literature [79]. At 2937 cm⁻¹, stretched C-H bond was formed which in turn sudden rises with immobilization of TiO₂. There were some notable changes in the spectrum of 2804–1700 cm⁻¹ and 1600–1000 cm⁻¹ can be due to the interaction between Ti-C or Ti: Fe [80]. After immobilization of iron nanoparticles in the nanofiber, the absorption peak imposed to dissociated carboxylic acid groups

at 1716 cm^{-1} disappeared and was substituted by a new strong band at 1560 cm^{-1} attributed to C=O stretching in the carboxylate. Changes at $800\text{--}1400\text{ cm}^{-1}$, in the region of $1380\text{--}1140\text{ cm}^{-1}$ (C–O stretching) and $980\text{--}850\text{ cm}^{-1}$ are evidence of interactions between iron nanoparticles and carboxyl groups. These results clearly establish successful immobilization of TiO_2 and Fe^0 nanoparticles in the surface of the nanofibers.

3.3 Thermogravimetric analysis

Poor thermal stability of nanofibers considers as one of the main drawbacks of much industrial application. The thermal behavior of the untreated and functionalized nanofibers was studied by TG analysis as shown in Fig. 3. It can be seen that immobilization of metal nanoparticles increases the thermal stability of nanofibrous mats. The visible decrease in mass weight was registered in three mass loss regions located around $60\text{--}100\text{ }^\circ\text{C}$, $250\text{--}300\text{ }^\circ\text{C}$ and $400\text{--}500\text{ }^\circ\text{C}$. The first weight loss region below $100\text{ }^\circ\text{C}$ can be explained by the evaporation of superficial water present in the sample while the other regions might be associated to the decomposition of the fiber constituents, and are related to the degradation of polymers. The weight loss around $250\text{--}300\text{ }^\circ\text{C}$ is due to the polymer degradation of PAA/PVA nanofibrous mats. However, at the elevated temperature around $400\text{--}500\text{ }^\circ\text{C}$, the polymer component of nanofibrous mats was disappeared, and the metal iron (Fe^0) and titanium dioxide (TiO_2) were left. The remaining weight percentage of functionalized nanofibrous mat is higher than that of untreated PAA/PVA mat evident the successful immobilization of metal nanoparticles in the surface of the nanofibers as illustrated in Scheme 3.

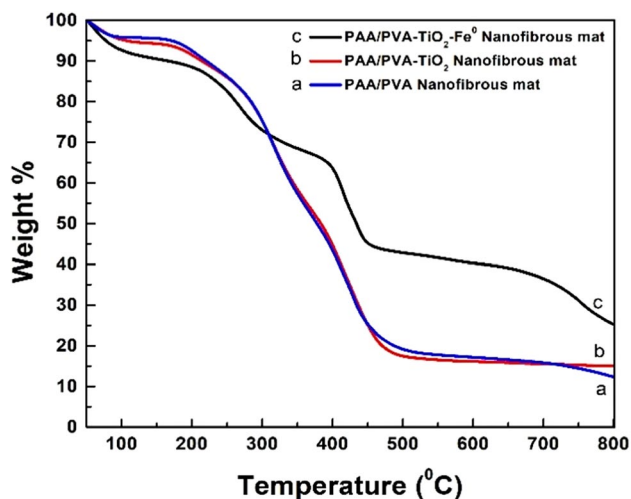
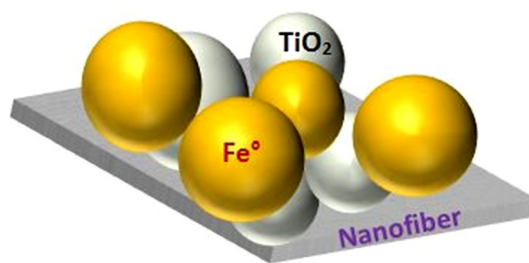


Fig. 3 TGA analysis of untreated and functionalized PAA/PVA nanofibrous mat



Scheme 3 Schematic illustration of immobilization of TiO_2 and Fe^0 nanoparticles

Based on remaining weight percentages, the amount of TiO_2 and Fe^0 nanoparticles incorporated in the nanofibers mat has been calculated as summarized in Table 2. It was summarized that about 2.62% TiO_2 nanoparticles were deposited in the surface of the PAA/PVA– TiO_2 nanofibrous mats, whereas 10.3% metal nanoparticles (both TiO_2 – Fe^0) has been incorporated in PAA/PVA– TiO_2 – Fe^0 , thus PAA/PVA– TiO_2 – Fe^0 showed higher thermal stability compared to PAA/PVA– TiO_2 could be due to thin layer immobilization through ion exchange instead of physical adsorption which is consistent to the literature [55]. However, the amount of iron and titanium could be tuned by variation in successive layer or metal nanoparticles [81, 82]. Consequently, the size of the TiO_2 and iron nanoparticles could also be extended through increasing the number of TiO_2 loading along with successive Fe(III) ion reduction cycles.

3.4 Photocatalytic degradation of dyes

The catalytic activities of PAA/PVA– TiO_2 and PAA/PVA– TiO_2 – Fe^0 nanofibrous mats were evaluated via monitoring their photocatalytic degradation of MB and BG dyes. The degradation experiment of both dyes was carried out under the same conditions. The UV spectroscopic analysis of dye degradation is shown in Fig. 4. It can be seen from Fig. 4a and b that, the characteristic absorption peak of MB at 630 nm has disappeared within 15 min and 20 min under UV-light irradiation with PAA/PVA– TiO_2 – Fe^0 and PAA/PVA– TiO_2 respectively. In Figure 4c and d, on the other hand, displays that the nanofibrous mat immobilized by metal nanoparticles can effectively degrade BG (625 nm) dyes within 10 min using

Table 2 Quantitative analysis of metal nanoparticles immobilized in PAA/PVA nanofibrous mats

| | PAA/PVA– TiO_2 | PAA/PVA– TiO_2 – Fe^0 |
|-----------------------------------|-------------------------|---|
| % Metal nanoparticles immobilized | 2.62 | 10.30 |

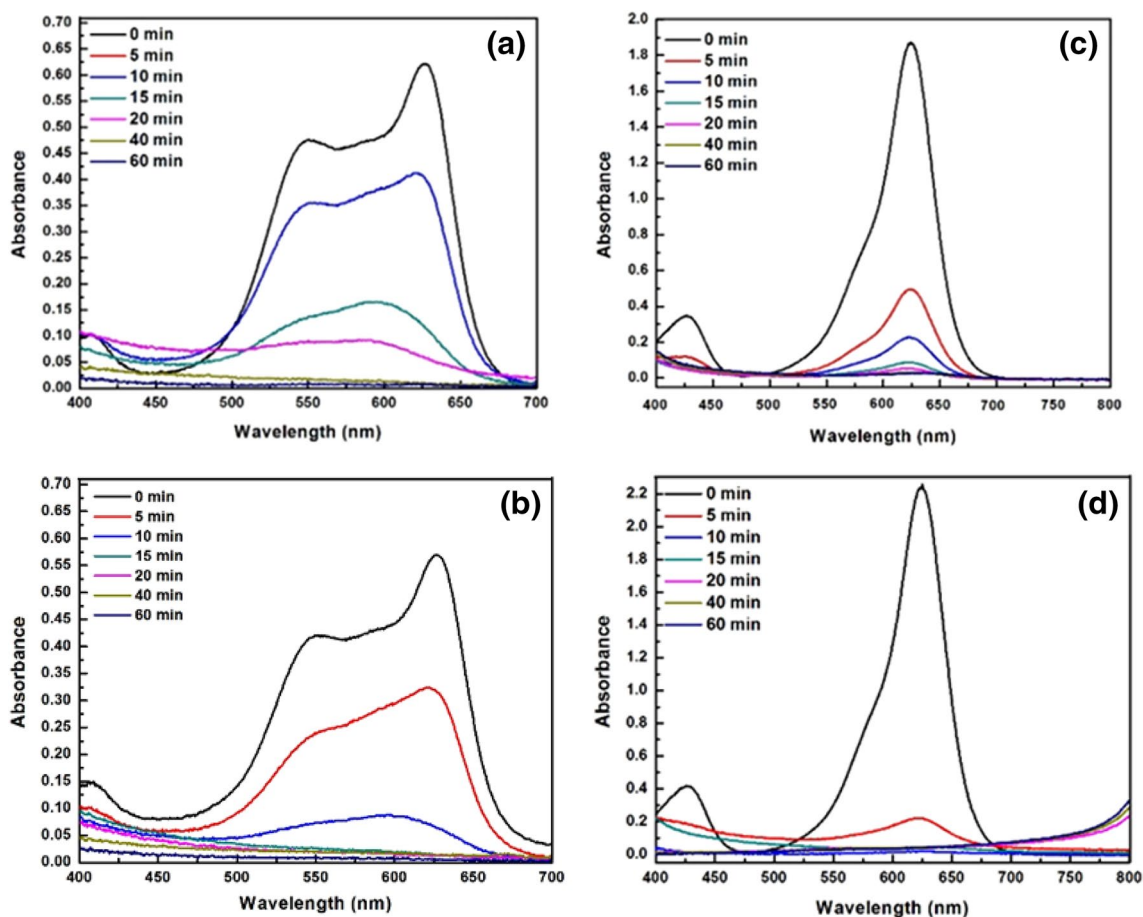


Fig. 4 UV-Vis absorption spectra for degradation of MB (a, b) and BG dyes (c, d) using PAA/PVA-TiO₂ and PAA/PVA-TiO₂-Fe⁰ nanofibrous mat as a photocatalyst, respectively [Reaction conditions: MB = 30 mg/L, BG = 60 mg/L, Mass catalyst = 500 mg/L; UV irradiation]

PAA/PVA-TiO₂-Fe⁰ as a photocatalyst, whereas PAA/PVA-TiO₂ showed complete degradation of BG by 20 min under UV light. Quicker degradation for both dyes was recorded in PAA/PVA-TiO₂-Fe⁰ nanofibrous mat can be due to the presence of ZVI NPs that prevented the recombination of hole-electron which ensures the oxidizing capacity of TiO₂.

3.4.1 Kinetics of degradation of individual dyes

Degradation kinetics is an important characteristic that represents the efficiency of bulk applications [83]. It is of great interest that PAA/PVA-TiO₂ and PAA/PVA-TiO₂-Fe⁰ nanofibrous mat demonstrated complete degradation of MB and BG dyes, as shown in Fig. 5a and b. The rate of degradation and the degradation reactions found to follow pseudo-first-order reaction kinetics, confirmed through previous reports [55, 71, 84, 85]. The [instant /initial] absorbance ratio (A_t/A_0) of band at 630 nm for MB and 625 nm for BG which accounts for the

corresponding concentration ratio (C_t/C_0), allows plotting $\ln(C_t/C_0)$ as a function of time (Fig. 5c-f) according to Eq. (5).

$$\ln \frac{C_t}{C_0} = \ln \frac{A_t}{A_0} - k \cdot t \quad (5)$$

Model validation of the first order kinetics for dye degradation with the catalyst is obtained by the linear evolution in time of $\ln(C/C_0)$, more particularly for functionalized nanofibrous mats, as supported by R^2 values beyond 0.98. Table 3 summarizes the catalytic kinetic plots of the PAA/PVA nanofibrous mat after and before the functionalization. All the plots show good linear relationship of $\ln(C_t/C_0)$ versus reaction time and follow pseudo-first-order kinetics. The rate constant for the degradation of dyes by PAA/PVA-TiO₂ was found to be 0.0645 min⁻¹ and 0.0705 min⁻¹ for MB and BG respectively; and by PAA/PVA-TiO₂-Fe⁰, the rate constant for the degradation of MB and BG was found 0.0847 min⁻¹ and 0.0989 min⁻¹ respectively. The best catalytic activity is registered for PAA/PVA-TiO₂-Fe⁰, which

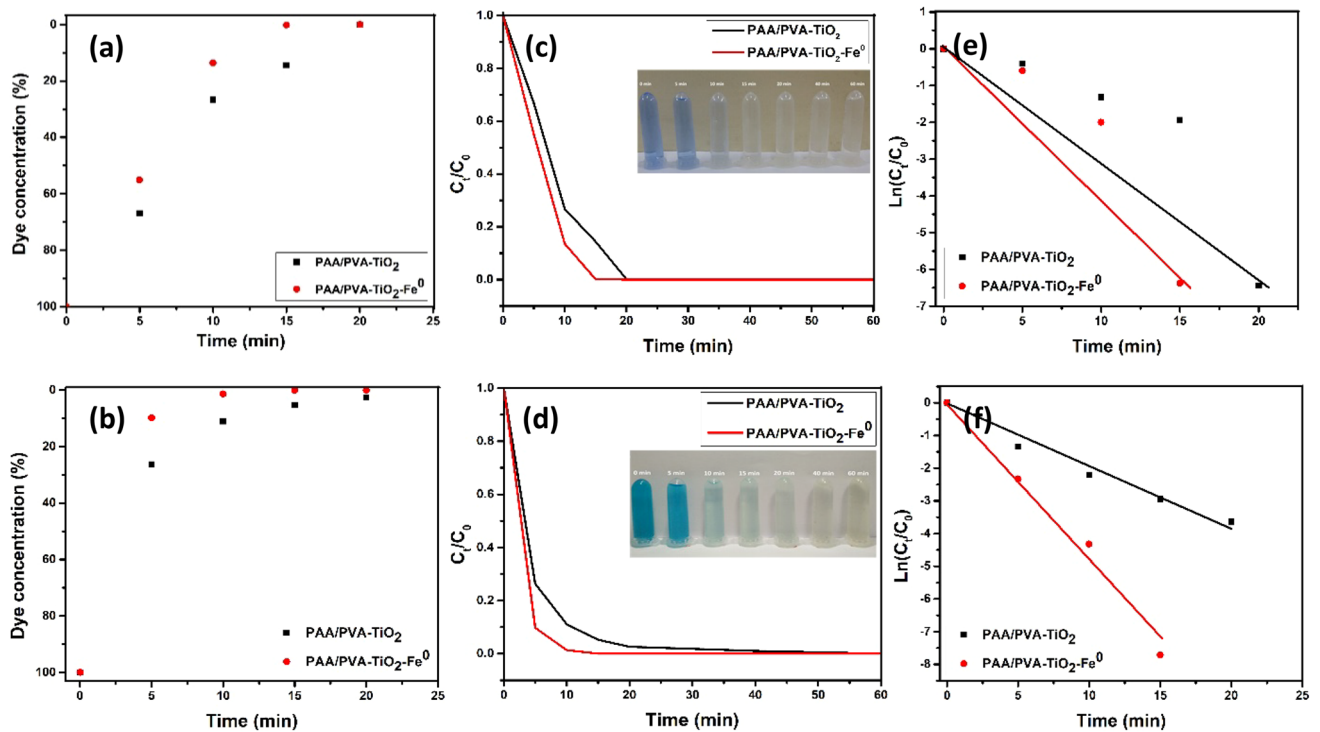


Fig. 5 Evolution of the conversion (a, b), C_t/C_0 (c, d) and $\ln(C_t/C_0)$ (e, f) versus time at room temperature of MB and BG degradation, respectively

Table 3 Kinetics study for the photocatalytic degradation of MB and BG dyes

| Nanofibrous mat | Time (min) | MB | | Time (min) | BG | |
|---|------------|------------------------|----------|------------|------------------------|----------|
| | | $K(\text{min}^{-1})^a$ | R^{2b} | | $K(\text{min}^{-1})^a$ | R^{2b} |
| PAA/PVA | 60 | – | – | 60 | – | – |
| PAA/PVA–TiO ₂ | 20 | 0.0645 | 0.9686 | 20 | 0.0705 | 0.9758 |
| PAA/PVA–TiO ₂ –Fe ⁰ | 15 | 0.0847 | 0.9731 | 10 | 0.0989 | 0.9854 |

^a K is the rate constant for the 1st order kinetics and is expressed in min^{-1}

^b R^2 is the correlation coefficient of the linear regression

Table 4 A comparison of the kinetic reaction constant for the photocatalytic degradation of dyes using PAA/PVA–TiO₂, PAA/PVA–TiO₂–Fe⁰ and other catalysts

| Pollutant Name | Samples | Concentration of dyes (mg/L) | k (min^{-1}) | Time (min) | Number of reusability cycles | References |
|----------------|--|------------------------------|---------------------------|------------|------------------------------|------------|
| MB | SnS | 1400 | 0.0220 | 120 | – | [86] |
| | Au@TiO ₂ | 13 | 0.0026 | 12 | 3 | [87] |
| | UVA/TiO ₂ | 20 | 0.121 | 180 | – | [32] |
| | Fe ₂ O ₃ /TiO ₂ | 25 | – | 180 | 3 | [88] |
| | PAA/PVA–TiO ₂ | 30 | 0.0645 | 20 | 4 | This work |
| | PAA/PVA–TiO ₂ –Fe ⁰ | 30 | 0.0847 | 15 | 4 | This work |
| BG | TiO ₂ /Zn | 4 | – | 180 | – | [89] |
| | Sr-doped TiO ₂ | 25 | – | 60 | – | [90] |
| | Ag ₈ SnS ₆ | 10 | 0.0036 | 90 | – | [91] |
| | Ni doped SnO ₂ /D65 | 5 | 0.0169 | 105 | – | [92] |
| | PAA/PVA–TiO ₂ | 60 | 0.0705 | 20 | 4 | This work |
| | PAA/PVA–TiO ₂ –Fe ⁰ | 60 | 0.0989 | 10 | 4 | This work |

can be attributed to the presence of ZVI NPs, as supported by a higher K .

Interestingly, many previous investigations reported more time to achieve more or less complete degradation of MB and BG dyes by photocatalysis as compared with our catalyst as shown in Table 4. Such rapid kinetics in degradation of MB and BG dyes might be attributed to the appreciable stability, dispersity and crosslink between PAA/PVA nanofibers and $\text{TiO}_2\text{-Fe}^0$ nanoparticles, ensuring the maximum exposure of active sites for dye degradation. For a control examination, degradation reaction using PAA/PVA nanofiber was also carried out. However, no degradation of dyes was observed which further evidence the effectiveness of $\text{TiO}_2\text{-Fe}^0$ nanoparticles towards degradation of MB and BG dyes.

3.4.2 Photocatalytic degradation of a mixture of dyes

Pollutants in the environment mostly found in mixed with other pollutants. Effluent from the different textile and printing industries contain several kinds of dyes in common wastewater which is difficult to treat through a general treatment facility. Removal of mixed pollutants is a great challenge towards complete detoxification of wastewater. The catalytic activity of prepared PAA/PVA- TiO_2 and PAA/PVA- $\text{TiO}_2\text{-Fe}^0$ nanofibrous mats towards degradation of a mixture of dyes was investigated as shown in Fig. 6.

An aqueous mixture of dye solution gives a strong absorption peak at 628 nm which represents both MB (630 nm) and BG (625 nm). Figure 6a shows a substantial decrease of absorbance 625 nm (BG) within 5 min during photocatalytic degradation of mixed pollutant solution using PAA/PVA- TiO_2 . After the disappearance of BG

dyes, MB was slowly degrading. 72% of pollutants have been removed in 60 min. This result is of great importance, which demonstrates the hard conversion of MB dyes. On the other hand, PAA/PVA- $\text{TiO}_2\text{-Fe}^0$ showed complete degradation of mixed dye solution within 60 min of UV irradiation which is consistent with the results discussed earlier.

3.5 Durability and stability of functional PAA/PVA nanofibrous mat

One of the great importance of PAA/PVA nanofibrous mat is the possibility of recovered and reused in consecutive degradation cycles which leads to the potentiality as a useful catalyst. For the commercial application of the catalysts, it is necessary to ensure adequate reusability to facilitate the cost-effectiveness of the technology. In the present work, we studied the reusability of PAA/PVA- TiO_2 and PAA/PVA- $\text{TiO}_2\text{-Fe}^0$ towards multiple cycle degradation of MB and BG under the same experimental protocol. Typically the catalysts were separated by simple separation methods, washed with distilled water and dried at a mild temperature before use in another cycle. The results indicate that both functional PAA/PVA nanofibrous mats are capable to be recycled and reused more than four (4) consecutive times without obvious decline in conversion processes (see Fig. 7) which opens a great prospect of nanofibers based photocatalyst for the potential industrial application.

In this case, the $\text{TiO}_2\text{-Fe}^0$ -immobilized fibrous mats are quite stable and can be easily isolated from the contaminated water. Even the Fe and TiO_2 NPs associated with polymeric fibrous mats do not disperse in the solution. SEM of further exposed to water for more than a month

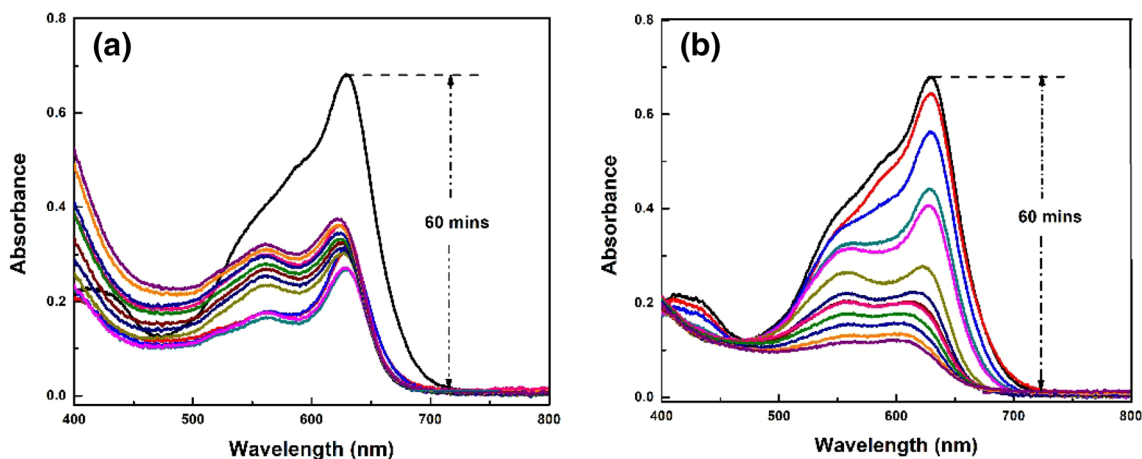


Fig. 6 UV-Vis absorption spectra for degradation of MB and BG dyes in mixed solutions using PAA/PVA- TiO_2 (a) and PAA/PVA- $\text{TiO}_2\text{-Fe}^0$ (b) nanofibrous mat as a photocatalyst

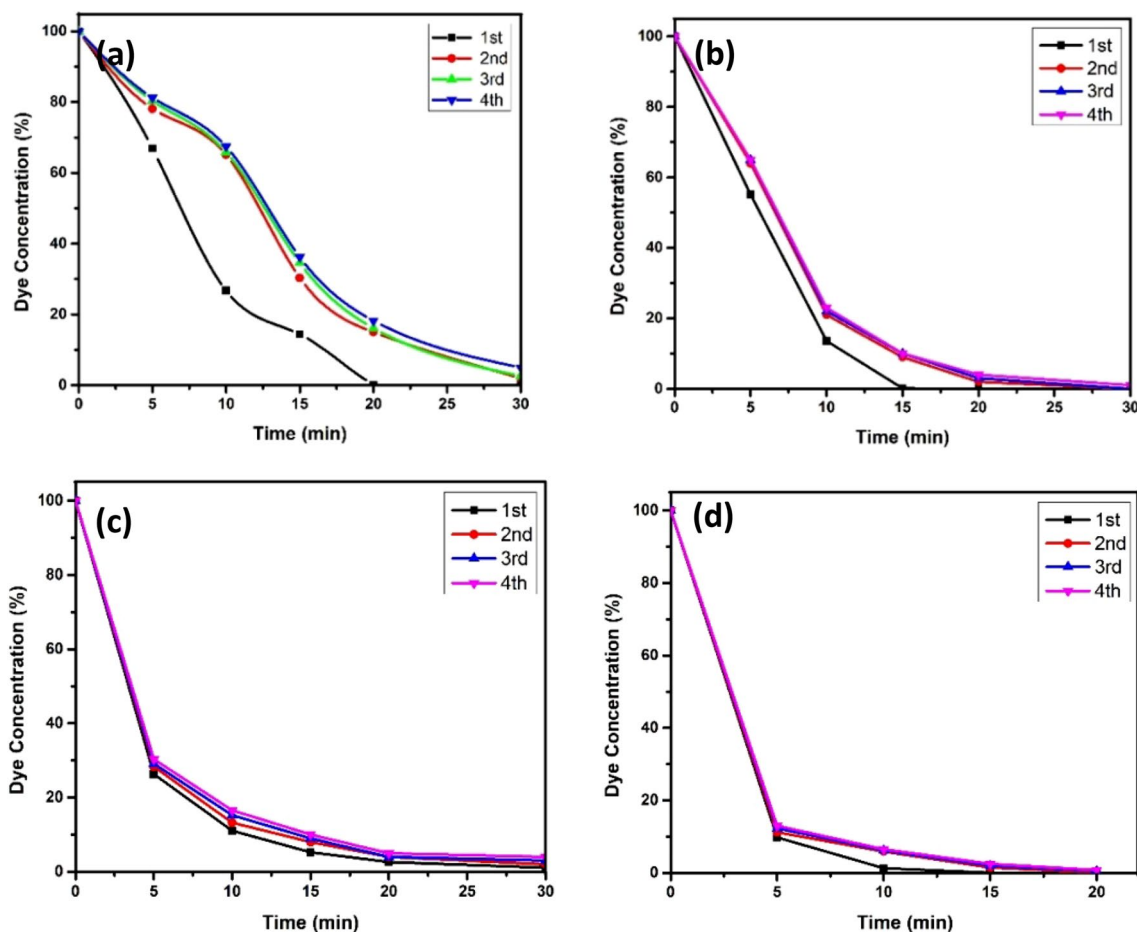


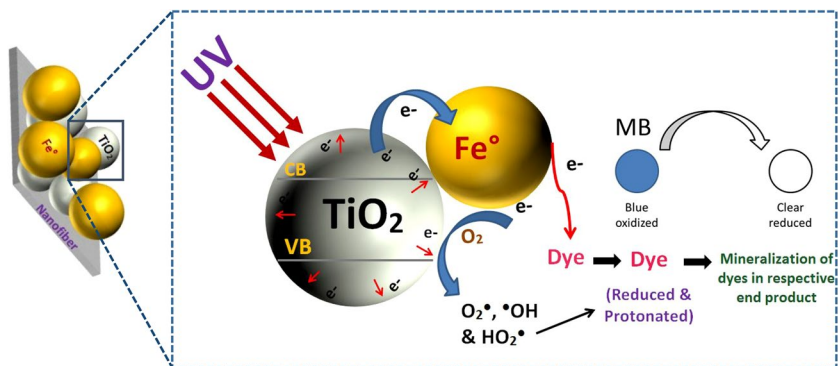
Fig. 7 Recyclability analysis of PAA/PVA–TiO₂ and PAA/PVA–TiO₂–Fe⁰ towards degradation of MB (a, b) and BG (c, d) respectively

showed no significant changes occurred. This validates the ability of the developed polyelectrolyte polymeric nanofibrous mats suitable for environmental applications. In this study, we planned to develop a system to expose fibrous mats in water for degradation experiment and it demonstrated the capability of this composited fibrous mat for environmental remediation.

3.6 The postulated mechanism for the catalytic degradation

As mentioned above, the changes of photocatalytic activity attributed to the reactive nature of excited nTiO₂ in presence of UV light [31]. The postulated mechanism for the photocatalytic degradation of MB and BG is presented

Scheme 4 Postulated mechanism for the photocatalytic degradation of MB and BG using PAA/PVA–TiO₂ and PAA/PVA–TiO₂–Fe⁰ as photocatalyst



in Scheme 4. As known that, insertion of metal particles (such as Fe) with TiO_2 increases the catalytic activity. The photocatalysis of the system with UV irradiation was initiated by the excitation of electrons from the ground state. The acceptance of the TiO_2 electrons by Fe^0 prevented the recombination of hole-electron, which sustains the oxidizing capacity of TiO_2 [33, 93]. However, this basic photocatalysis mechanism involves the TiO_2 excitation under UV light from the ground state to the triplet-excited state [94]. Due to the reaction between these trapped electrons and dissolved oxygen in the system, superoxide (O_2^-) radical anions are formed which in turn result into hydroxyl radicals formation. These OH radicals are mainly responsible for the oxidation of the MB and BG into nontoxic substances [95].

4 Conclusion

In summary, this work was an exertion to develop a simplistic approach to a novel photo-catalyst by immobilization of $\text{TiO}_2\text{-Fe}^0$ nanoparticles in PAA/PVA nanofibrous mats. Resultant nanofibrous mats found to capable of catalyzing the photocatalytic degradation of hazardous dyes (MB and BG) with a degradation efficiency of 99.5%. It has shown a great interest in the application of such nanofibrous composite for various novel applications. The experiment of the photocatalytic application after immobilization of different metallic, organic and inorganic polymers to PAA/PVA composite nanofibers are ongoing in the laboratory. Furthermore, this project generated that as prepared PAA/PVA polymer nanofibrous mats can be useful in the removal of many other contaminants from wastewater and opening a new arena for fabrication of different inorganic/organic materials for versatile smart application. In our future efforts, we will develop the composited nonwoven mats as membrane filtration materials, which are expected to be used conveniently for remediation of diverse contaminants in wastewater.

References

1. C. Singh, A. Goyal, S. Singhal, Nickel-doped cobalt ferrite nanoparticles: efficient catalysts for the reduction of nitroaromatic compounds and photo-oxidative degradation of toxic dyes. *Nanoscale* **6**, 7959–7970 (2014)
2. C. Fernández, M.S. Larrechi, M.P. Callao, An analytical overview of processes for removing organic dyes from wastewater effluents. *TrAC Trends Anal. Chem.* **29**, 1202–1211 (2010)
3. P. Kovacic, R. Somanathan, Nitroaromatic compounds: environmental toxicity, carcinogenicity, mutagenicity, therapy and mechanism. *J. Appl. Toxicol.* **34**, 810–824 (2014)
4. H.-Y. Xu, W.-C. Liu, J. Shi, H. Zhao, S.-Y. Qi, Photocatalytic discoloration of Methyl Orange by anatase/schorl composite: optimization using response surface method. *Environ. Sci. Pollut. Res.* **21**, 1582–1591 (2014)
5. J. Cao, C. Zhou, H. Lin, B. Xu, S. Chen, Direct hydrolysis preparation of plate-like BiOI and their visible light photocatalytic activity for contaminant removal. *Mater. Lett.* **109**, 74–77 (2013)
6. S. Sharma, R. Ameta, R. Malkani, S.C. Ameta, Use of semi-conducting bismuth sulfide as a photocatalyst for degradation of Rose Bengal. *Maced. J. Chem. Chem. Eng.* **30**, 229–234 (2011)
7. N. Muhd Julkapli, S. Bagheri, S. Bee Abd, Hamid, Recent advances in heterogeneous photocatalytic decolorization of synthetic dyes. *Sci. World J.*, **2014**, 25 (2014)
8. S.-Y. Lee, S.-J. Park, TiO_2 photocatalyst for water treatment applications. *J. Ind. Eng. Chem.* **19**, 1761–1769 (2013)
9. B. Sambandam, A. Surejan, L. Philip, T. Pradeep, Rapid synthesis of C– TiO_2 : tuning the shape from spherical to rice grain morphology for visible light photocatalytic application. *ACS Sustain. Chem. Eng.* **3**, 1321–1329 (2015)
10. F. Lüddecke, S. Heß, C. Gallert, J. Winter, H. Güde, H. Löffler, Removal of total and antibiotic resistant bacteria in advanced wastewater treatment by ozonation in combination with different filtering techniques. *Water Res.* **69**, 243–251 (2015)
11. X. Qu, J. Brame, Q. Li, P.J. Alvarez, Nanotechnology for a safe and sustainable water supply: enabling integrated water treatment and reuse. *Accounts Chem. Res.* **46**, 834–843 (2012)
12. M. Khajeh, S. Laurent, K. Dastafkan, Nanoadsorbents: classification, preparation, and applications (with emphasis on aqueous media). *Chem. Rev.* **113**, 7728–7768 (2013)
13. M. Liu, J. Zheng, Q. Liu, S. Xu, M. Wu, Q. Xue, Z. Yan, H. Xiao, Z. Wei, H. Zhu, The preparation, load and photocatalytic performance of N-doped and CdS-coupled TiO_2 . *RSC Adv.* **3**, 9483–9489 (2013)
14. P. Guo, L.T. Meng, C.H. Wang, Core-shell WO_3/TiO_2 nanorod heterostructures for solar light photocatalysis. *Adv. Mater. Res.* **850**, 78–81 (2014)
15. K. Ullah, S. Ye, L. Zhu, Z.-D. Meng, S. Sarkar, W.-C. Oh, Microwave assisted synthesis of a noble metal-graphene hybrid photocatalyst for high efficient decomposition of organic dyes under visible light. *Mater. Sci. Eng. B* **180**, 20–26 (2014)
16. R. Adhikari, G. Gyawali, S.H. Cho, R. Narro-García, T. Sekino, S.W. Lee, $\text{Er}^{3+}/\text{Yb}^{3+}$ co-doped bismuth molybdate nanosheets upconversion photocatalyst with enhanced photocatalytic activity. *J. Solid State Chem.* **209**, 74–81 (2014)
17. J.G. McEvoy, W. Cui, Z. Zhang, Synthesis and characterization of Ag/AgCl—activated carbon composites for enhanced visible light photocatalysis. *Appl. Catal. B* **144**, 702–712 (2014)
18. A. Azzouz, S. Nousir, N. Bouazizi, R. Roy, Metal–inorganic–organic matrices as efficient sorbents for hydrogen storage. *ChemSusChem* **8**, 800–803 (2015)
19. N. Bouazizi, F. Ajala, M. Khelil, H. Lachheb, K. Khirouni, A. Houas, A. Azzouz, Zinc oxide incorporating iron nanoparticles with improved conductance and capacitance properties. *J. Mater. Sci.* **27**, 11168–11175 (2016)
20. N. Bouazizi, R. Bargougui, P. Thebault, T. Clamens, F. Desriac, F. Fiorese, G. Ladam, S. Morin-Grognet, N. Mofaddel, O. Lesouhaitier, Development of a novel functional core-shell-shell nanoparticles: from design to anti-bacterial applications. *J. Coll. Interface Sci.* **513**, 726–735 (2018)
21. B. Nabil, N.M. Mohammad, N. Behary, C. Christine, V. Julien, O. Thoumire, A. Abdelkrim, Development of new multifunctional filter based nonwovens for organics pollutants reduction and detoxification: high catalytic and antibacterial activities. *Chem. Eng. J.* **356**, 702–716 (2018)
22. N. Bouazizi, A. El achari, C. Campagne, J. Vieillard, A. Azzouz, Copper oxide coated polyester fabrics with enhanced catalytic properties towards the reduction of 4-nitrophenol. *J. Mater. Sci.* **29**, 1–12 (2018)

23. J.-L. Gong, B. Wang, G.-M. Zeng, C.-P. Yang, C.-G. Niu, Q.-Y. Niu, W.-J. Zhou, Y. Liang, Removal of cationic dyes from aqueous solution using magnetic multi-wall carbon nanotube nanocomposite as adsorbent. *J. Hazard. Mater.* **164**, 1517–1522 (2009)
24. J. Peralta-Hernández, Y. Meas-Vong, F.J. Rodríguez, T.W. Chapman, M.I. Maldonado, L.A. Godínez, Comparison of hydrogen peroxide-based processes for treating dye-containing wastewater: decolorization and destruction of Orange II azo dye in dilute solution. *Dyes Pigm.* **76**, 656–662 (2008)
25. O. Carp, C.L. Huisman, A. Reller, Photoinduced reactivity of titanium dioxide. *Prog. Solid State Chem.* **32**, 33–177 (2004)
26. X. Zhang, L. Lei, J. Zhang, Q. Chen, J. Bao, B. Fang, A novel CdS/S-TiO₂ nanotubes photocatalyst with high visible light activity. *Sep. Purif. Technol.* **66**, 417–421 (2009)
27. P.V. Bedja, Kamat, Capped semiconductor colloids. synthesis and photoelectrochemical behavior of TiO₂ capped SnO₂ nanocrystallites. *J. Phys. Chem.* **99**, 9182–9188 (1995)
28. D.J. Norris, A.L. Efros, S.C. Erwin, Doped nanocrystals. *Science* **319**, 1776–1779 (2008)
29. R. Ali, S.H. Hassan, Degradation studies on paraquat and malathion using TiO₂/ZnO based photocatalyst. *Malaysian J. Anal. Sci.* **12**, 77–87 (2008)
30. K. Soutsas, V. Karayannis, I. Poullos, A. Riga, K. Ntampegliotis, X. Spiliotis, G. Papapolymerou, Decolorization and degradation of reactive azo dyes via heterogeneous photocatalytic processes. *Desalination* **250**, 345–350 (2010)
31. M. Rauf, S.S. Ashraf, Fundamental principles and application of heterogeneous photocatalytic degradation of dyes in solution. *Chem. Eng. J.* **151**, 10–18 (2009)
32. R. Dariani, A. Esmaeili, A. Mortezaali, S. Dehghanpour, Photocatalytic reaction and degradation of methylene blue on TiO₂ nano-sized particles. *Optik* **127**, 7143–7154 (2016)
33. J. Arana, O.G. Díaz, M.M. Saracho, J.D. Rodríguez, J.H. Melián, J.P. Peña, Photocatalytic degradation of formic acid using Fe/TiO₂ catalysts: the role of Fe³⁺/Fe²⁺ ions in the degradation mechanism. *Appl. Catal. B* **32**, 49–61 (2001)
34. H. Měšť'ánková, G. Mailhot, J. Jirkovský, J. Krýsa, M. Bolte, Mechanistic approach of the combined (iron–TiO₂) photocatalytic system for the degradation of pollutants in aqueous solution: an attempt of rationalisation. *Appl. Catal. B* **57**, 257–265 (2005)
35. A.-G. Rincón, C. Pulgarin, Comparative evaluation of Fe³⁺ and TiO₂ photoassisted processes in solar photocatalytic disinfection of water. *Appl. Catal. B* **63**, 222–231 (2006)
36. Y. Yu, C.Y. Jimmy, J.-G. Yu, Y.-C. Kwok, Y.-K. Che, J.-C. Zhao, L. Ding, W.-K. Ge, P.-K. Wong, Enhancement of photocatalytic activity of mesoporous TiO₂ by using carbon nanotubes. *Appl. Catal. A* **289**, 186–196 (2005)
37. F. He, D. Zhao, Manipulating the size and dispersibility of zerovalent iron nanoparticles by use of carboxymethyl cellulose stabilizers. *Environ. Sci. Technol.* **41**, 6216–6221 (2007)
38. W. Zhang, C.-B. Wang, H.-L. Lien, Treatment of chlorinated organic contaminants with nanoscale bimetallic particles. *Catal. Today* **40**, 387–395 (1998)
39. B. Schrick, J.L. Blough, A.D. Jones, T.E. Mallouk, Hydrodechlorination of trichloroethylene to hydrocarbons using bimetallic nickel–iron nanoparticles. *Chem. Mater.* **14**, 5140–5147 (2002)
40. Y.-H. Tee, E. Grulke, D. Bhattacharyya, Role of Ni/Fe nanoparticle composition on the degradation of trichloroethylene from water. *Indus. Eng. Chem. Res.* **44**, 7062–7070 (2005)
41. J. Xu, D. Bhattacharyya, Membrane-based bimetallic nanoparticles for environmental remediation: Synthesis and reactive properties. *Environ. Prog.* **24**, 358–366 (2005)
42. Y. Xu, W. Zhang, Subcolloidal Fe/Ag particles for reductive dehalogenation of chlorinated benzenes. *Ind. Eng. Chem. Res.* **39**, 2238–2244 (2000)
43. P. Varanasi, A. Fullana, S. Sidhu, Remediation of PCB contaminated soils using iron nano-particles. *Chemosphere* **66**, 1031–1038 (2007)
44. C.-B. Wang, W.-X. Zhang, Synthesizing nanoscale iron particles for rapid and complete dechlorination of TCE and PCBs. *Environ. Sci. Technol.* **31**, 2154–2156 (1997)
45. S.R. Kanel, J.-M. Greneche, H. Choi, Arsenic (V) removal from groundwater using nano scale zero-valent iron as a colloidal reactive barrier material. *Environ. Sci. Technol.* **40**, 2045–2050 (2006)
46. S.M. Ponder, J.G. Darab, T.E. Mallouk, Remediation of Cr(VI) and Pb(II) aqueous solutions using supported, nanoscale zero-valent iron. *Environ. Sci. Technol.* **34**, 2564–2569 (2000)
47. X. Li, D.G. Brown, W. Zhang, Stabilization of biosolids with nanoscale zero-valent iron (nZVI). *J. Nanopart. Res.* **9**, 233–243 (2007)
48. W.J. Epolito, H. Yang, L.A. Bottomley, S.G. Pavlostathis, Kinetics of zero-valent iron reductive transformation of the anthraquinone dye Reactive Blue 4. *J. Hazard. Mater.* **160**, 594–600 (2008)
49. J. Fan, Y. Guo, J. Wang, M. Fan, Rapid decolorization of azo dye methyl orange in aqueous solution by nanoscale zerovalent iron particles. *J. Hazard. Mater.* **166**, 904–910 (2009)
50. J.G. Darab, A.B. Amonette, D.S. Burke, R.D. Orr, S.M. Ponder, B. Schrick, T.E. Mallouk, W.W. Lukens, D.L. Caulder, D.K. Shuh, Removal of pertechnetate from simulated nuclear waste streams using supported zerovalent iron. *Chem. Mater.* **19**, 5703–5713 (2007)
51. G. Naja, A. Halasz, S. Thiboutot, G. Ampleman, J. Hawari, Degradation of hexahydro-1, 3, 5-trinitro-1, 3,5-triazine (RDX) using zerovalent iron nanoparticles. *Environ. Sci. Technol.* **42**, 4364–4370 (2008)
52. G. Kim, W. Jeong, S. Choe, Dechlorination of atrazine using zero-valent iron (Fe⁰) under neutral pH conditions. *J. Hazard. Mater.* **155**, 502–506 (2008)
53. N.M. Mahmoodi, M. Arami, Degradation and toxicity reduction of textile wastewater using immobilized titania nanophotocatalysis. *J. Photochem. Photobiol. B* **94**, 20–24 (2009)
54. A.K. Ray, A.A. Beenackers, Novel photocatalytic reactor for water purification. *AIChE J.* **44**, 477–483 (1998)
55. H. Deb, S. Xiao, M.N. Morshed, S. Al Azad, Immobilization of cationic titanium dioxide (TiO₂⁺) on electrospun nanofibrous mat: synthesis, characterization, and potential environmental application. *Fibers Polymers* **19**, 1715–1725 (2018)
56. X. Wang, Y. Liu, Z. Hu, Y. Chen, W. Liu, G. Zhao, Degradation of methyl orange by composite photocatalysts nano-TiO₂ immobilized on activated carbons of different porosities. *J. Hazard. Mater.* **169**, 1061–1067 (2009)
57. Galperin, Dynamic mechanical properties of a TiO₂-filled crosslinked epoxy resin from 20 to 90 °C. *J. Appl. Polym. Sci.* **11**, 1475–1481 (1967)
58. E. Santala, M. Kemell, M. Leskelä, M. Ritala, The preparation of reusable magnetic and photocatalytic composite nanofibers by electrospinning and atomic layer deposition. *Nanotechnology* **20**, 035602 (2008)
59. N.N. Fathima, R. Aravindhan, J.R. Rao, B.U. Nair, Dye house wastewater treatment through advanced oxidation process using Cu-exchanged Y zeolite: a heterogeneous catalytic approach. *Chemosphere* **70**, 1146–1151 (2008)
60. H. Sassi, G. Lafaye, H. Ben Amor, A. Gannouni, M.R. Jeday, J. Barbier, Wastewater treatment by catalytic wet air oxidation process over Al-Fe pillared clays synthesized using microwave irradiation. *Front. Environ. Sci. Eng.* **12**, 2 (2018)

61. J. Li, C. Liu, Y. Liu, Au/graphene hydrogel: synthesis, characterization and its use for catalytic reduction of 4-nitrophenol. *J. Mater. Chem.* **22**, 8426–8430 (2012)
62. A. Shukla, R.K. Singha, T. Sasaki, R. Bal, Nanocrystalline Pt–CeO₂ as an efficient catalyst for a room temperature selective reduction of nitroarenes. *Green Chem.* **17**, 785–790 (2015)
63. Z. Jiang, D. Jiang, W. Wei, Z. Yan, J. Xie, Natural carbon nanodots assisted development of size-tunable metal (Pd, Ag) nanoparticles grafted on bionic dendritic α -Fe₂O₃ for cooperative catalytic applications. *J. Mater. Chem. A* **3**, 23607–23620 (2015)
64. H.-L. Jiang, B. Liu, T. Akita, M. Haruta, H. Sakurai, Q. Xu, Au@ZIF-8: CO oxidation over gold nanoparticles deposited to metal–organic framework. *J. Am. Chem. Soc.* **131**, 11302–11303 (2009)
65. H.-L. Jiang, T. Akita, T. Ishida, M. Haruta, Q. Xu, Synergistic catalysis of Au@Ag core–shell nanoparticles stabilized on metal–organic framework. *J. Am. Chem. Soc.* **133**, 1304–1306 (2011)
66. E. Mirzadeh, K. Akhbari, Synthesis of nanomaterials with desirable morphologies from metal–organic frameworks for various applications. *CrystEngComm* **18**, 7410–7424 (2016)
67. M. Jahan, Z. Liu, K.P. Loh, A Graphene oxide and copper-centered metal organic framework composite as a tri-functional catalyst for HER, OER, and ORR. *Adv. Func. Mater.* **23**, 5363–5372 (2013)
68. A. Dhakshinamoorthy, M. Opanasenko, J. Čejka, H. Garcia, Metal organic frameworks as heterogeneous catalysts for the production of fine chemicals. *Catal. Sci. Technol.* **3**, 2509–2540 (2013)
69. Y. Zhao, D.-S. Deng, L.-F. Ma, B.-M. Ji, L.-Y. Wang, A new copper-based metal–organic framework as a promising heterogeneous catalyst for chemo- and regio-selective enamination of β -ketoesters. *Chem. Commun.* **49**, 10299–10301 (2013)
70. N. Bhardwaj, S.C. Kundu, Electrospinning: a fascinating fiber fabrication technique. *Biotechnol. Adv.* **28**, 325–347 (2010)
71. S. Xiao, X. Luo, Q. Peng, H. Deb, Effective removal of calcium ions from simulated hard water using electrospun polyelectrolyte nanofibrous mats. *Fibers Polymers* **17**, 1428–1437 (2016)
72. S. Xiao, M. Shen, R. Guo, Q. Huang, S. Wang, X. Shi, Fabrication of multiwalled carbon nanotube-reinforced electrospun polymer nanofibers containing zero-valent iron nanoparticles for environmental applications. *J. Mater. Chem.* **20**, 5700–5708 (2010)
73. S. Xiao, M. Shen, R. Guo, S. Wang, X. Shi, Immobilization of zerovalent iron nanoparticles into electrospun polymer nanofibers: synthesis, characterization, and potential environmental applications. *J. Phys. Chem. C* **113**, 18062–18068 (2009)
74. L. Li, Y.-L. Hsieh, Ultra-fine polyelectrolyte hydrogel fibres from poly (acrylic acid)/poly (vinyl alcohol). *Nanotechnology* **16**, 2852 (2005)
75. K. Kumeta, I. Nagashima, S. Matsui, K. Mizoguchi, Crosslinking reaction of poly (vinyl alcohol) with poly (acrylic acid)(PAA) by heat treatment: effect of neutralization of PAA. *J. Appl. Polym. Sci.* **90**, 2420–2427 (2003)
76. W. He, Z. Ma, T. Yong, W.E. Teo, S. Ramakrishna, Fabrication of collagen-coated biodegradable polymer nanofiber mesh and its potential for endothelial cells growth. *Biomaterials* **26**, 7606–7615 (2005)
77. J. Zeng, H. Hou, J.H. Wendorff, A. Greiner, Electrospun poly (vinyl alcohol)/poly (acrylic acid) fibres with excellent water-stability. *e-polymers*, **4**, 1 (2004)
78. H. Ma, Y. Huang, M. Shen, D. Hu, H. Yang, M. Zhu, S. Yang, X. Shi, Enhanced decoloration efficacy of electrospun polymer nanofibers immobilized with Fe/Ni bimetallic nanoparticles. *RSC Adv.* **3**, 6455–6465 (2013)
79. S. Xiao, S. Wu, M. Shen, R. Guo, Q. Huang, S. Wang, X. Shi, Polyelectrolyte multilayer-assisted immobilization of zero-valent iron nanoparticles onto polymer nanofibers for potential environmental applications. *ACS Appl. Mater. Interfaces* **1**, 2848–2855 (2009)
80. M.N. Morshed, X. Shen, H. Deb, S.A. Azad, X. Zhang, R. Li, Sonochemical fabrication of nanocrystalline titanium dioxide (TiO₂) in cotton fiber for durable ultraviolet resistance. *J. Nat. Fibers*, (2018) <https://doi.org/10.1080/15440478.2018.1465506>
81. T.C. Wang, M.F. Rubner, R.E. Cohen, Polyelectrolyte multilayer nanoreactors for preparing silver nanoparticle composites: controlling metal concentration and nanoparticle size. *Langmuir* **18**, 3370–3375 (2002)
82. X. Zhang, H. Wang, Z. Su, Fabrication of Au@Ag core–shell nanoparticles using polyelectrolyte multilayers as nanoreactors. *Langmuir*, **28**, 15705–15712 (2012)
83. M. Li, Q. Gao, T. Wang, Y.-S. Gong, B. Han, K.-S. Xia, C.-G. Zhou, Solvothermal synthesis of Mn_xFe_{3-x}O₄ nanoparticles with interesting physicochemical characteristics and good catalytic degradation activity. *Mater. Des.* **97**, 341–348 (2016)
84. S.K. Ghosh, M. Mandal, S. Kundu, S. Nath, T. Pal, Bimetallic Pt–Ni nanoparticles can catalyze reduction of aromatic nitro compounds by sodium borohydride in aqueous solution. *Appl. Catal. A* **268**, 61–66 (2004)
85. N. Bouazizi, J. Vieillard, R. Bargougui, N. Couvrat, O. Thoumire, S. Morin, G. Ladam, N. Mofaddel, N. Brun, A. Azzouz, Entrapment and stability of iron nanoparticles within APTES modified graphene oxide sheets with improved catalytic activity. *J. Alloys Compd.* **771**, 1090–1102 (2018)
86. F. Jamali-Sheini, R. Yousefi, N.A. Bakr, M. Cheraghizade, M. Sookhajian, N.M. Huang, Highly efficient photo-degradation of methyl blue and band gap shift of SnS nanoparticles under different sonication frequencies. *Mater. Sci. Semicond. Process.* **32**, 172–178 (2015)
87. M.M. Khan, J. Lee, M.H. Cho, Au@TiO₂ nanocomposites for the catalytic degradation of methyl orange and methylene blue: an electron relay effect. *J. Ind. Eng. Chem.* **20**, 1584–1590 (2014)
88. R. Li, Y. Jia, N. Bu, J. Wu, Q. Zhen, Photocatalytic degradation of methyl blue using Fe₂O₃/TiO₂ composite ceramics. *J. Alloy. Compd.* **643**, 88–93 (2015)
89. S. Munusamy, R. sai laxmi Aparna, R. Gunneswara Subramanya Vara Prasad, Photocatalytic effect of TiO₂ and the effect of dopants on degradation of brilliant green. *Sustain. Chem. Process.* **1**, 4 (2013)
90. S. Sood, A. Umar, S.K. Mehta, A. Sinha, S.K. Kansal, Efficient photocatalytic degradation of brilliant green using Sr-doped TiO₂ nanoparticles. *Ceram. Int.* **41**, 3533–3540 (2015)
91. B.H. Shambharkar, A.P. Chowdhury, Ethylene glycol mediated synthesis of Ag₈SnS₆ nanoparticles and their exploitation in the degradation of eosin yellow and brilliant green. *RSC Adv.* **6**, 10513–10519 (2016)
92. S. Ragupathy, T. Sathya, Photocatalytic decolorization of brilliant green by Ni doped SnO₂ nanoparticles. *J. Mater. Sci.* **29**, 8710–8719 (2018)
93. B. Tryba, Immobilization of TiO₂ and Fe–TiO₂ photocatalysts on the cotton material for application in a flow photocatalytic reactor for decomposition of phenol in water. *J. Hazard. Mater.* **151**, 623–627 (2008)
94. S. Weiren, Z. Wenkuan, H. Fei, F. Youling, TiO₂ based photocatalysis and its applications for waste water treatment. *Prog. Chem.* (1998). <https://doi.org/10.1155/2013/319637>
95. N. Xu, Z. Shi, Y. Fan, J. Dong, J. Shi, M.Z.-C. Hu, Effects of particle size of TiO₂ on photocatalytic degradation of methylene blue in aqueous suspensions. *Indus. Eng. Chem. Res.* **38**, 373–379 (1999)